Journal of Quantitative Spectroscopy & Radiative Transfer 176 (2016) 34–49

Contents lists available at ScienceDirect

Journal of Quantitative Spectroscopy & Radiative Transfer

journal homepage: www.elsevier.com/locate/jqsrt

Elevated aerosol layers modify the O_2–O_2 absorption measured by ground-based MAX-DOAS

Ivan Ortega [a,b], Larry K. Berg [c], Richard A. Ferrare [d], Johnathan W. Hair [d], Chris A. Hostetler [d], Rainer Volkamer [a,b,*]

[a] Department of Chemistry and Biochemistry, University of Colorado, Boulder, CO, USA
[b] Cooperative Institute for Research in Environmental Sciences (CIRES), Boulder, CO, USA
[c] Pacific North West National Laboratory, Richland, WA, USA
[d] NASA Langley Research Center, Hampton, VA, USA

ARTICLE INFO

Article history:
Received 8 October 2015
Received in revised form
15 February 2016
Accepted 16 February 2016
Available online 22 February 2016

Keywords:
DOAS
Oxygen collisional complex (O_4)
O_4 correction factor (CF_{O4})
Aerosol extinction profiles
Elevated aerosol layers

ABSTRACT

The oxygen collisional complex (O_2–O_2, or O_4) is a greenhouse gas, and a calibration trace gas used to infer aerosol and cloud properties by Differential Optical Absorption Spectroscopy (DOAS). Recent reports suggest the need for an O_4 correction factor (CF_{O4}) when comparing simulated and measured O_4 differential slant column densities (dSCD) by passive DOAS. We investigate the sensitivity of O_4 dSCD simulations at ultraviolet (360 nm) and visible (477 nm) wavelengths towards separately measured aerosol extinction profiles. Measurements were conducted by the University of Colorado 2D-MAX-DOAS instrument and NASA's multispectral High Spectral Resolution Lidar (HSRL-2) during the Two Column Aerosol Project (TCAP) at Cape Cod, MA in July 2012. During two case study days with (1) high aerosol load (17 July, AOD ~ 0.35 at 477 nm), and (2) near molecular scattering conditions (22 July, AOD < 0.10 at 477 nm) the measured and calculated O_4 dSCDs agreed within 6.4 ± 0.4% (360 nm) and 4.7 ± 0.6% (477 nm) if the HSRL-2 profiles were used as input to the calculations. However, if in the calculations the aerosol is confined to the surface layer (while keeping AOD constant) we find $0.53 < CF_{O4} < 0.75$, similar to previously reported CF_{O4}. Our results suggest that elevated aerosol layers, unless accounted for, can cause negative bias in the simulated O_4 dSCDs that can explain CF_{O4}. The air density and aerosol profile aloft needs to be taken into account when interpreting the O_4 from ground-based MAX-DOAS. Opportunities to identify and better characterize these elevated layers are also discussed.

1. Introduction

The collision-induced absorption of oxygen (O_2–O_2, or O_4) absorbs solar radiation at multiple bands throughout the ultraviolet (UV), visible and near-infrared regions of the electromagnetic spectrum [1,2]. O_2–O_2 has no bound state at atmospherically relevant temperatures, and its concentration in the atmosphere is proportional to the square of the oxygen concentration. Hence it can be predicted with little error (< 0.1%) if the temperature and pressure profiles are known [2]. Analysis of the strong absorption bands of O_4 provides a unique way to characterize how clouds and aerosols modify the photon trajectories, therefore providing informing about cloud-top pressure, effective cloud coverage, and aerosol optical properties. In particular, O_4 is being used extensively as an atmospheric reference gas in Differential Optical Absorption Spectroscopy (DOAS) applications,

* Corresponding author at: Department of Chemistry and Biochemistry, University of Colorado, 215 UCB, Boulder, CO 80309, USA.
Tel.: +1 303 492 1843.
E-mail address: rainer.volkamer@colorado.edu (R. Volkamer).

http://dx.doi.org/10.1016/j.jqsrt.2016.02.021
0022-4073/

including Multi Axis DOAS (MAX-DOAS) [3–6], airborne MAX-DOAS [7–9], in-situ DOAS instruments [2,10], and satellites [11]. Since most of the O_4 is located below 4 km, the analysis of O_4 is particularly useful to infer aerosol and cloud properties in the lowermost part of the troposphere.

Trace gas profiles derived from passive DOAS techniques, i.e., MAX-DOAS and airborne MAX-DOAS, require aerosol extinction profiles as prerequisite information in radiative transfer models (RTM). The vertical sensitivity of the measurements to perturbations in the species of interest is quantified by the weighting functions, which for optically thin absorbers such as O_4 are the same as the box-air mass factor (bAMF) [12]. The weighting functions are calculated with RTMs by the ratio of the partial slant column density (SCD) to the partial vertical column density (VCD) contained in an atmospheric layer. Retrieval algorithms based on nonlinear inversion such as optimal estimation need the weighting functions [13]. If the photon path trajectory in the RTM is well-constrained by knowledge of the aerosol extinction, then the error in the weighting functions decreases; consequently, the final error of the trace gas inversion also decreases. By contrast, assumptions about aerosol extinction profiles can lead to considerable errors. In this context, O_4 observations are important because they yield information about the extinction profiles [3,4]. Over the past few years, many ground-based MAX-DOAS observations have reported O_4 dSCDs that exceed those simulated by RTM. An O_4 correction factor (CF_{O4}) was applied to improve the correlation of simulated and measured O_4 differential AMF (dAMF or differential SCD, dSCD; differential with regards to the amount contained in the reference spectrum) [5,14–18]. The cause of this CF_{O4} is currently not understood. Recent airborne and direct-sun DOAS testing of O_4 dSCDs did not find a need for CF_{O4} [9,19]. However, the CF_{O4} values reported by ground-based MAX-DOAS vary between different studies, see Table 1, and CF_{O4} is consistently needed at low AOD ($<$ 0.2 at 360 nm) [5,14] and/or at high AOD (up to 1.5 at 477 nm) [15–18]. Past MAX-DOAS studies that needed CF_{O4} have either lacked independent measurements of vertically resolved extinction profiles, and/or made simplifying assumptions about the aerosol extinction profiles, i.e., confining aerosols to the near the surface (within the boundary layer (BL), see Table 1).

Uncertainties in the temperature and pressure dependencies of O_4 cross sections had been suggested as possible causes for the CF_{O4} [5,14]. Recently, laboratory measurements of the O_4 absorption cross sections have quantified the temperature dependence of the spectral band shape for a variety of bands at ultraviolet and visible wavelengths (Thalman and Volkamer [2]). The O_4 bands at 360 and 477 nm have further been reproduced from field observations in a Rayleigh atmosphere within narrow error bounds ($<$3% error) [19]. This error is significantly smaller than the 25 ± 10% differences reported in the literature (see Table 1). Furthermore, Volkamer et al. [9] compared modeled and measured O_4 dSCDs from airborne MAX-DOAS, and reconciled the inferred aerosol extinction profile with independent aerosol extinction profiles retrieved by High Spectral Resolution LIDAR (HSRL) over a wide range of conditions. They did not need CF_{O4} different from unity over the full range of altitudes probed (0–14.5 km). Some recent evaluations of ground-based MAX-DOAS have used qualitative information about aerosol vertical distributions (e.g., Irie et al. [18]; Remmers and Wagner [20]). To our knowledge only airborne MAX-DOAS has been evaluated using quantitative vertically-resolved aerosol profiles [9]. In this work, we study the effect of simplifying assumptions about aerosol profiles on O_4 dSCDs, and assess the validity of these assumptions using independent measurements of highly-resolved aerosol extinction profiles using the data from NASA's HSRL-2 instrument aboard the B200 aircraft deployment as part of the first phase of the Department of Energy (DOE) Two Column Aerosol Project (TCAP) [21].

2. Methodology

The first intensive phase of the TCAP field campaign took place in the east coast of North America (over Cape Cod, MA, U.S.) through July and part of August 2012. The primary TCAP objectives were to characterize the aerosol direct effect under polluted conditions (over Cape Cod, MA), and contrast it with pristine conditions several hundred kilometers away from land over the Atlantic Ocean. Here we use data collected at the DOE Atmosphere Radiation Measurement (ARM) Mobile Facility (AMF) site with the 2-D-MAX-DOAS located at the Highlands Center in the Cape Cod National Seashore about 85 km southeast of Boston, MA and aboard the NASA B-200 King Air aircraft with the second generation HSRL-2 (Fig. 1). Details about the comprehensive set of measurements aboard aircrafts and with DOE Atmospheric Radiation Measurement (ARM) Mobile Facility located at the base of the Cape Cod are described in Berg et al. [21]. We present results for two distinctive cloud-free days with very different AOD conditions and when the King Air aircraft carried out overpasses above the TCAP ground site (Tuesday 17 July and Sunday 22 July 2012). Fig. 1 shows the NASA's King Air flight tracks on both days.

2.1. The 2-D-MAX-DOAS instrument and O_4 retrieval

The 2-D-MAX-DOAS instrument, including the retrieval of range-resolved NO_2 (3-D distributions), are described in detail in Ortega et al. [22]. Briefly, the 2-D-MAX-DOAS instrument as deployed during TCAP consisted of three synchronized spectrograph/detector units located indoors in a temperature-controlled sea container and the control measurement laptop; the 2-D telescope was mounted outdoors on the railing of the seatainer ($\sim$45 m ASL, above sea level), providing an unobstructed view close to the horizon towards 0 and 180° azimuth angles (AA) relative to north. The 2-D measurements during TCAP provide a unique data set to test and validate diurnal spatial distribution of AOD and aerosol microphysical properties, which are part of a separate study. In this work, we use off-axis scans that consisted of seven elevation angles (EA) (1°, 3°, 6°, 8°, 10°, 20°, 45° above the horizon, and zenith) and the two AAs. The integration time for spectra recorded at each EA was 1 min. The scattered light collected with the

Table 1
Previous ground-based MAX-DOAS using the CF_{O4}.

Reference	Wavelength (nm)	AOD	Aerosol Profile information[a]	CF_{O4}
Wagner et al. [14]	360	0.1–0.2	NO[b]	~ 0.78
Clémer et al. [5]	360, 477, 577, 630	< 0.15 (360 nm)	NO[c]	0.75
Irie et al. [15]	360, 477	0.1–1.0	NO[d]	0.75
Vlemmix et al. [16]	477	0.1–0.8	NO[e]	0.80
Zieger et al. [17]	360, 477	0.1–0.8	Qualitative[f]	~0.80[g]
Irie et al. [18]	476	0.1–1.5	Qualitative[h]	~0.83[i]

[a] Indicating whether highly resolved aerosol extinction profiles (BL and free troposphere) were available and/or used in the simulation of O_4.

[b] Aerosol profile approximated as box-profile, i.e., constant extinction between the surface and 1 km.

[c] CF_{O4} was determined using elevation angles of 15° and 30°; aerosol profile assumption: exponential decrease with a scale-height of 0.5 km, AOD as measured by a co-located Sun photometer.

[d] Aerosol extinction retrieval; assumes exponential decrease in the lowest 1 km.

[e] Similar approach as in [5].

[f] Raman lidar (355 nm); assumes a backscatter to extinction ratio between 60 m and 750 m; above 750 m the lidar ratio was determined and multiplied with the backscatter signal to obtain extinction profiles (200 m resolution).

[g] Average CF_{O4} applied to four participating MAX-DOAS during the CINDI campaign.

[h] Aerosol extinction in the BL was inferred by lidar, assuming a constant lidar ratio; lidar extinctions in the BL were compared with independent in-situ and MAX-DOAS retrievals. MAX-DOAS extinctions profiles were retrieved by modifying profile shapes in 1 km thick layers below 3 km constrained by partial AODs.

[i] Calculated with the empirical off-axis scan dependent CF_{O4} to a set of elevation angles ($\leq 10°$); in this case 10°.

2-D telescope was focused into a single CeramOptics 25 m × 1.0 mm silica mono-fiber coupled to a tri-furcated fiber bundle connected to three Ocean Optics (QE6500) spectrometers with a wavelength range between 300 and 631 nm with a spectral resolution between 0.4 and 0.6 nm (FWHM).

The spectra collected at each EA were analyzed using the DOAS method [23] and the WinDOAS software package [24]. Details about the retrieval of O_4 dSCDs in the UV and visible, as well as the cross sections that were fitted simultaneously are listed in Table 2. All the high-resolution trace gas cross sections were adjusted to the instrumental resolution using the slit functions determined close to the fit window by means of mercury emission lines. The zenith sky spectra recorded at the start of each EA scan is used as reference spectrum to evaluate the O_4 dSCDs from the other EAs. A Ring cross section is calculated from the respective reference spectrum using the DOASIS software [31] and included in the fit to account for the "filling in" of Fraunhofer lines due to rotational Raman scattering [14,32]. An example spectrum of the DOAS analysis of O_4 at 360 and 477 nm is shown in Fig. 2. We refer to the O_4 dSCDs retrieved over the spectral ranges 338–370 nm and 438–488 nm as the O_4 dSCDs at 360 and 477 nm, respectively, using the wavelength of the maximum peak absorptions in the UV and visible respectively (see Table 2). We estimate upper limit O_4 dSCD errors of about 7% ($\sim 1.80 \times 10^{42}$ molec^2/cm^5) for 360 nm and 4% ($\sim 1.45 \times 10^{42}$ molec^2/cm^5) for 477 nm. These errors are estimated as the overall variation in O_4 dSCD from sensitivity tests that used different O_4 cross sections [2,33], wavelength windows, and polynomial order according with past studies [5,9]. In general, the O_4 dSCD variations are about 8 times the DOAS fit error calculated internally in WinDOAS as the standard deviations on the retrieved dSCD [24].

The time series of O_4 dSCDs is shown for two cloud-free days, i.e., 17 and 22 July 2012, in Fig. 3. The top panels A and C show the dSCDs at 360 nm, and the bottom panels B and D show the dSCDs at 477 nm. The magnitude and EA dependence of the measured O_4 dSCDs on both days are quite different and serve to inform qualitatively on atmospheric and AOD conditions. On 17 July the small O_4 dSCDs in the low EAs indicate high AOD. For comparison, the clear splitting and higher O_4 dSCDs along the different EAs on 22 July indicate lower AOD. In general, the instrument horizontal distance sensitivity is enhanced for low AOD. The aerosol extinction profiles and the AOD are examined in Section 2.2. The yellow shaded areas in Fig. 3 represent the periods of time when two overpasses were carried out with the NASA King Air above the TCAP ground site and that were used to simulate and compare the O_4 dSCDs.

2.2. The High Spectral Resolution Lidar – 2 (HSRL-2)

The HSRL-2, an improved version of the airborne HSRL-1 instrument [34], measures profiles of particle backscatter coefficients and linear particle depolarization ratios at 355, 532, and 1064 nm; and particle volume extinction coefficients at 355 and 532 nm [35]. During TCAP, data were sampled at 100 m horizontal and 15 m vertical resolutions using the nadir-viewing geometry below the aircraft. The aircraft altitude was about 8 km above ground level during all flights. Hair et al. [34] describes the determination of 532 nm aerosol extinction coefficient from the measured power in the molecular channel. The molecular extinction is calculated from modeled density profiles. The calculation of aerosol extinction is only performed where the overlap function is unity (approximately 2.5 km from the aircraft). The 355 nm aerosol extinction is computed in a similar manner. To avoid ground return issues, the extinction profiles start at about 165 m above the surface. Below this altitude we assume homogeneous mixing of aerosols and use a constant extinction values measured at 165 m. For detailed information about the HSRL-2 instrument and the TCAP deployment, see Muller et al. [36]. Fig. 1 shows the NASA's King Air flight tracks close to the ground site on the two selected days.

Fig. S1 in the supporting information shows the curtain aerosol extinction profiles at 532 nm obtained on both days during the entire flight time, highlighting the overpasses above the ground site. We have averaged the HSRL-2 extinction profiles for segments when the aircraft was within 10 km radius of the 2-D-MAX-DOAS location (white circle of Fig. 1). The 10 km radius used to average the HSRL-2 captures well the horizontal path length realized

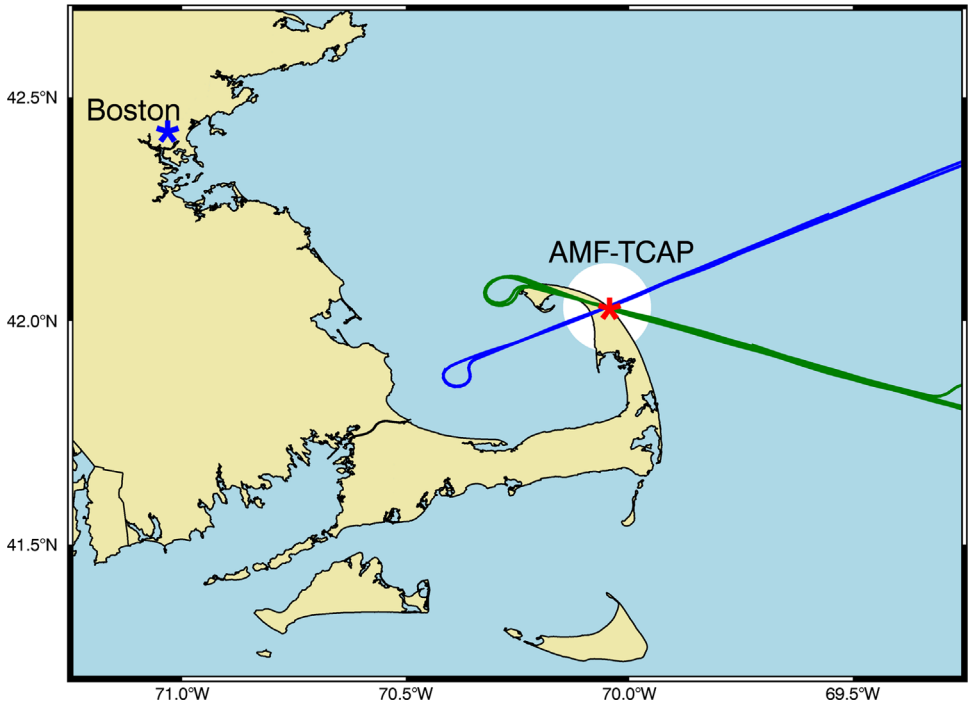

Fig. 1. Map of the Cape Cod Bay area. The TCAP ground-based site is shown with the red asterisk. The major city of Boston is shown with the blue asterisk. The NASA's King Air flight tracks on 17 and 22 July 2012 are indicated with the green and blue lines respectively. The white circle area represents the 10 km radius that is used to average the extinction profiles from the HSRL-2. (For interpretation of the references to color in this figure legend, the reader is referred to the web version of this article.)

Table 2
Summary of the DOAS fitting analysis of O_4 in the UV and visible.

Cross section	Fitting window		Reference
	O_4 (UV) 338–370 nm	O_4 (visible) 438–488 nm	
O_4 (293 K)	X	X	Thalman and Volkamer [2]
O_3 (223 K)	X		Bogumil et al. [25]
O_3 (243 K)	X	X	Bogumil et al. [25]
NO_2 (294 K)	X	X	Vandaele et al. [26]
H_2O HITEMP (294)		X	Rothman et al. [27]
CHOCHO		X	Volkamer et al. [28]
HCHO	X		Meller and Moortgat. [29]
BrO	X		Fleischmann et al. [30]
Ring	X	X	Kraus [31]
Additional information			
Polynomial	5	5	
Intensity offset	Linear (2 terms)		
RTM wavelength (nm)	360	477	

by the 2-D-MAX-DOAS, especially on 17 July when the path length calculated from the O_4 dSCDs and O_4 concentration ranges from ~9 km (360 nm) to 13 km (477 nm) for an EA of 6° [22]. On 22 July, the horizontal path length was greater due to smaller AOD, and ranged from 13 km (360 nm) to 19 km (477 nm) for an EA of 6°. However, the HSRL-2 aerosol extinction profile averaged over a radius of 20 km is very similar to that obtained with the 10 km radius. The difference in MAX-DOAS O_4 dSCDs obtained using the HSRL-2 aerosol extinction profile averaged over a radius of 20 km and over a radius of 10 km is about 0.1%. On 17 July the flight track was from southeast to northwest, returning by following a similar flight track after ~1.5 h. The first and second overpass time averages are at 11:35 and 13:00 LST. On 22 July the flight track was similar but from northeast to southwest at 12:12 LST with similar return track at 12:53 LST.

The averaged extinction profiles at 360 and 477 nm, where O_4 has strong absorption bands, were calculated using the extinction Angstrom exponent between the standard wavelengths of 355 and 532 nm. As an example, Fig. 4 shows the averaged aerosol extinction profiles at 360

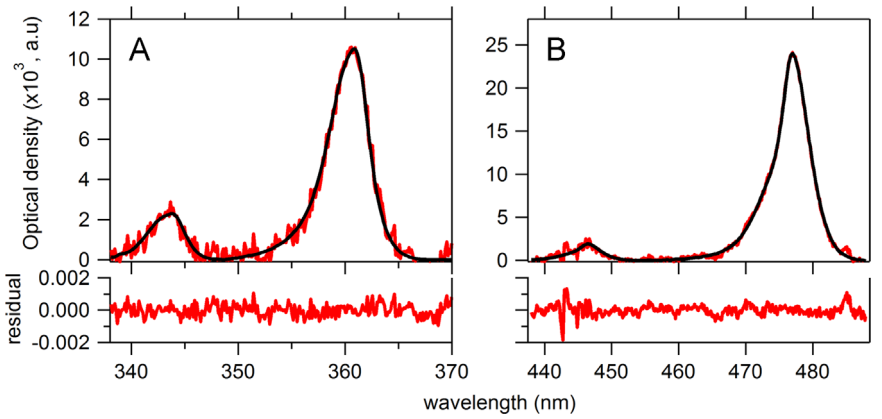

Fig. 2. Example of the O_4 fit in the UV and visible using the DOAS settings listed in Table 1. The example is from 17 July 2012 close in time to the NASA's King air overpass (about 11 LST, SZA=32, EA=3, and north AA). (A) O_4 analysis in the UV (360 nm). The RMS is 3.93×10^{-4} and the O_4 dSCD is 2.49×10^{43} molecules^2 cm^{-5}. (B) O_4 analysis in the UV (477 nm). The RMS is 3.29×10^{-4} and the O_4 dSCD is 3.65×10^{43} molecules^2 cm^{-5}. The red lines represent measured spectra and black lines are scaled reference cross sections. (For interpretation of the references to color in this figure legend, the reader is referred to the web version of this article.)

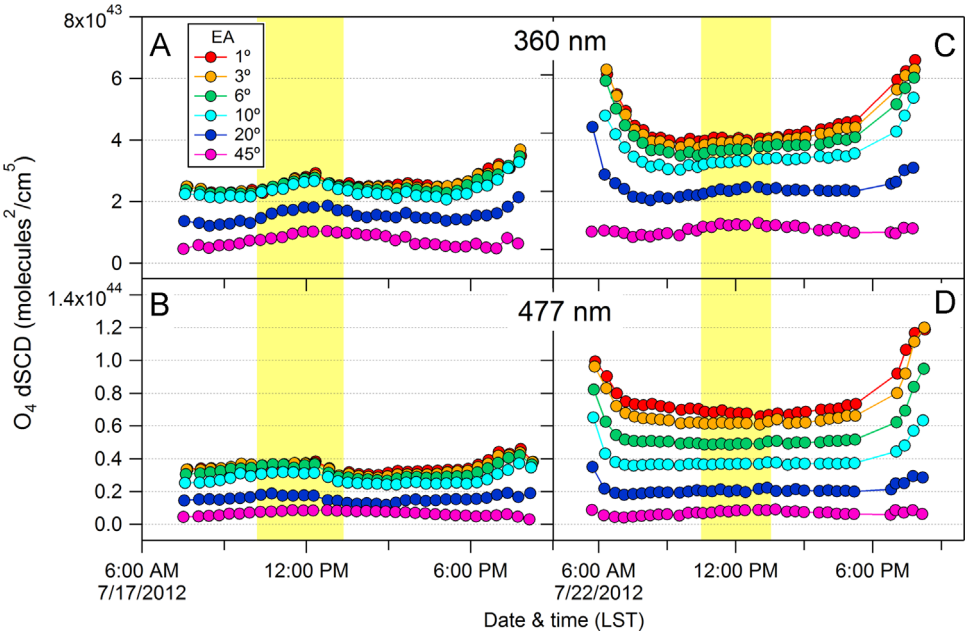

Fig. 3. Time series of the O_4 dSCDs obtained with the elevation angle scan on 17 July (A and B) and 22 July 2012 (C and D). The north AA is shown. The 360 and 477 nm are shown on top and bottom respectively. The yellow shaded areas characterize the period of time used to simulate and compare the O_4 dSCDs and where the NASA's King air carried out overpasses above the TCAP ground site. (For interpretation of the references to color in this figure legend, the reader is referred to the web version of this article.)

and 477 nm obtained during the second overpass on both days. On 17 July, the aerosol extinction was significantly higher than on 22 July as previously identified with the O_4 dSCDs. The inhomogeneity of AOD around the ground site was assessed by calculating the AOD below the aircraft altitude down to the surface from the profiles as observed when the airplane was on the west and east sides above the 2-D-MAX-DOAS measurement site within the same overpass (see Fig. 1). The average AOD at 477 nm during the first overpass (11:35 LST) on 17 July was 0.253 with a variability of 0.001 calculated as the difference between the AODs integrated from HSRL-2 extinction profiles measured towards the east and west of 2-D-MAX-DOAS site. The average AOD during the second overpass (13:00 LST) was 0.313 with a slightly higher variability of 0.045 between the east and west directions. On 22 July, the average AOD was 0.093 ($\pm$0.005) for the first overpass (12:12 LST) and 0.108 ($\pm$0.001) for the second overpass (12:53 LST). As can be seen, for most of the time homogeneity within 2% percent was identified, except on the second overpass on 17 July where AOD varied by about 10%. The molecular scattering using the method reported by Bodhaine et al. [37] is calculated at 360 and 477 nm to compare with the extinction profile as measured by the HSRL-2 (see Fig. 4). As can be seen on 17 July, the extinction due to the aerosols was consistently higher below

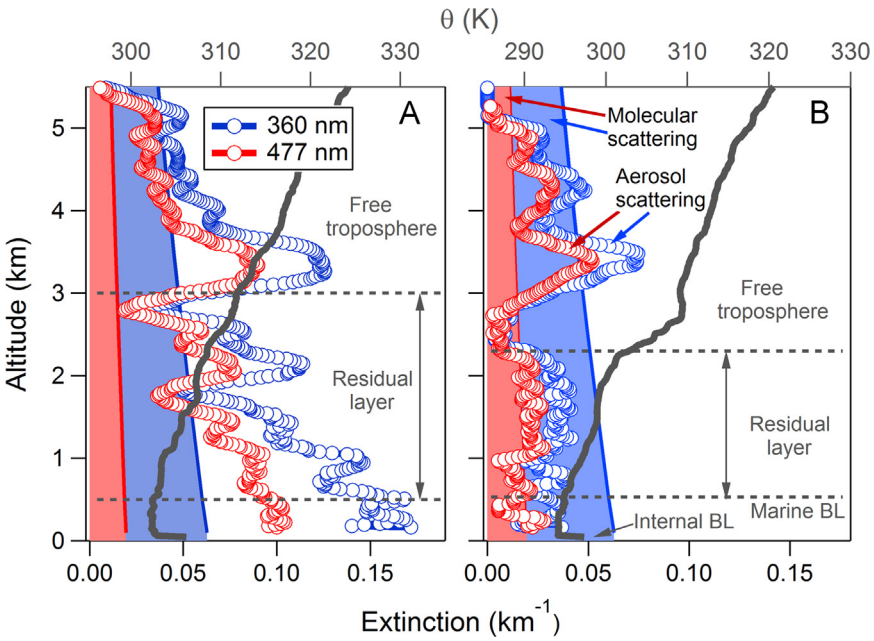

Fig. 4. Averaged HSRL-2 aerosol extinction profiles obtained during the overpasses on (A) 17 July 2012, and (B) 22 July 2012 (< 10 km radius). The filled area indicates extinction due to molecular scattering. The potential temperature (θ) profiles derived from radiosondes launched at the AMF site are shown in continuous gray lines. The dotted horizontal lines indicate the approximate altitude of the marine BL, residual layer, and free troposphere.

2 km. On the other hand, on 22 July the aerosol extinction below 2 km is very close to or even lower (especially for the 360 nm) than the molecular scattering.

Elevated aerosol layers were frequently observed during TCAP [21]. The potential temperature profile for both case study days is shown in Fig. 4 and reveals a relatively shallow marine BL (~400 m), an internal BL associated with warming of the Cape Cod peninsula (0–60 m), a decoupled residual layer above the mixed layer, and elevated aerosol layers in the free troposphere. For a detailed characterization of these elevated aerosol layers see Berg et al. [21]. Here, we use the potential temperature profiles to calculate partial AOD columns in the BL, residual layer, and in the free troposphere. The partial AOD contained in the free troposphere represented 32% (360 nm) and 36% (477 nm) on the first overpass and 35% (360 nm) and 36% (477 nm) during the second overpass on 17 July. On 22 July the partial AOD above 2 km were even higher: 51% (360 nm) and 56% (477 nm) for the first overpass and 56% (360 nm) and 61% (477 nm) for the second overpass.

2.3. Additional measurements

The additional suite of measurements used to complement our study are the atmospheric temperature and pressure profiles provided by the radiosondes, which were launched four times a day at the AMF site (~00, 05, 17, and 23 UTC). The vertical resolution of the sondes was about 10 m reaching a maximum altitude of about 28 km. For this study, the closest radiosonde in time (17 UTC or 13:00 LST) is used to construct the O_4 concentration profile and to prescribe the temperature, pressure and relative humidity in the RTM (see Section 2.4).

Further comparison of the AOD measured by HSRL-2 with ground-based multifilter rotating shadow band radiometer (MFRSR) [38], and a Cimel Sun photometer [39] showed good agreement, with AODs retrieved by the HSRL-2 generally being 5-10% smaller than the ground-based AOD, indicating that 90–95% of the aerosol extinction was indeed located below the aircraft. The small difference could be due to underestimation of the aerosols in the very shallow aerosol layer near the surface (< 165 m) where the HSRL-2 loses sensitivity (ground return), or due to aerosol extinction in layers located above the aircraft altitude of approximately 8 km.

2.4. Radiative Transfer Modeling

The simulation of the O_4 dSCDs was performed using the full spherical Monte-Carlo atmospheric radiative transfer model (McArtim) [40]. McArtim was initialized using the geometry of the EA scan performed with the 2-D-MAX-DOAS during TCAP. The altitude grid used in the radiative transfer calculations to forward model the O_4 dSCDs was set to 100 m thickness between 0 and 12 km, 1 km thickness between 12 and 25 km, and 2.5 km thickness between 25 and 100 km. The average aerosol extinction profile in 100 m thickness layers obtained with the HSRL-2 is used between 0 and 8 km to represent the air mass probed by the HSRL-2. The wavelengths chosen to forward model the O_4 dSCDs were 360 and 477 nm. Pressure and temperature profiles up to 28 km were taken from the radiosonde (Section 2.3) adjusted to this altitude grid. Above 28 km the U.S standard atmosphere was used. When the 2-D-MAX-DOAS was pointing towards the south, the land surface albedo obtained from atmospheric transmission by the co-located MFRSR [41] was used (0.04 at 360 nm, and 0.05 at 477 nm).

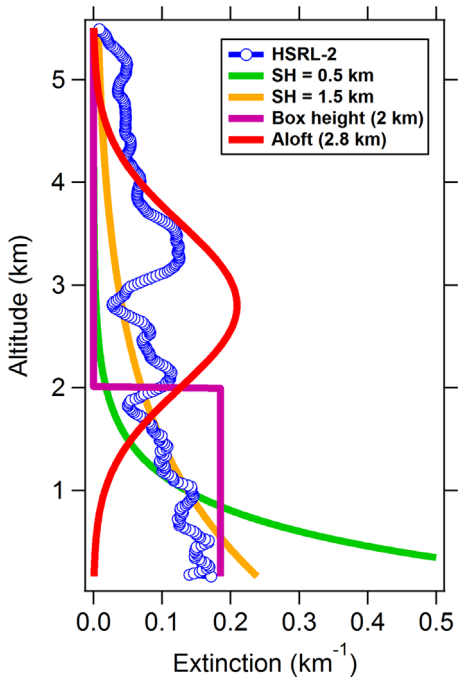

Fig. 5. Example of aerosol extinction profile shapes assumed at 360 nm to constrain the RTM. All the extinction profiles are constrained by the AOD obtained with the HSRL-2, i.e., all have the same AOD. In this example we used the extinction profile at 360 nm obtained on 17 July. (For interpretation of the references to color in this figure, the reader is referred to the web version of this article.)

When pointing to the north, which mostly sees the ocean; we assumed a Lambertian surface albedo of 0.07 for both wavelengths [42]. Additional aerosol optical parameters consisted of a single scattering albedo, ssa, of 0.98 [36], and the aerosol phase function represented by an asymmetry parameter, *g*, of 0.68 (Greenstein approximation), which are typical for this location [43]. We have conducted sensitivity studies that varied ssa ($\pm$ 0.05) and g ($\pm$ 0.05) and found a small effect ($<$2% total) on the simulation of O_4 dSCDs. Similar findings are presented in Clémer et al. [5] and Baidar et al. [8]. For the comparison with the measurements, RTM calculated O_4 SCDs of the zenith view were subtracted from SCDs at other elevation angles.

Sensitivity studies were further performed that varied the aerosol extinction profiles while keeping the AOD constant (constrained by HSRL-2). Fig. 5 shows the different aerosol extinction profiles created to test the sensitivity of simulated O_4 dSCDs. We use two aerosol profiles exponentially decreasing with altitude, one with a scale-height (SH) of 0.5 and the other with SH of 1.5 km (orange and green lines in Fig. 5); a homogeneous aerosol extinction profile with a height of 2 km was assumed to represent well-mixed homogeneous BL; and the red profile in Fig. 5 represents the extinction profile assumed to be aloft with a Gaussian shape. The maximum extinction of this profile is at 2.8 km and a width of 0.8 km. To compare with the real extinction profiles we also use the profiles retrieved with the HSRL-2 interpolated to the RTM grid vertical resolution.

3. Results and discussions

The sensitivity studies presented in Section 3.1 have in common that the AOD was constrained to that measured by HSRL-2, and the aerosol extinction profile shape was varied. In Section 3.2 we present additional sensitivity studies to further assess the influence of the elevated aerosol layers. In this case, the HSRL-2 aerosol extinction below 2 km was used, while the aerosol extinction above 2 km was set to zero. The following sections discuss TCAP results in context with the available literature about elevated aerosol layers (Section 3.3), CF_{O4} found with previous MAX-DOAS measurements (Section 3.4). Finally, Section 3.5 summarizes the need for future research and gives an Outlook.

3.1. Comparison of measured and simulated O_4 dSCDs

Fig. 6 shows the comparison of simulated and measured O_4 dSCDs for different EAs (3°-A; 6°-B; 10°-C; and 20°-D) at 477 nm. The data shown here represent both AAs, and both days. The four EAs were chosen to represent a range of low and high angles that are sensitive to the air masses probed by the HSRL-2. The different aerosol scenarios used during simulations are represented using the same color scheme as that of Fig. 5. Note that for clarity the axis scale is different for each EA. The light blue shaded area for the low EAs ($\leq 10°$) shows the values obtained on 17 July – high AOD. This clear split in the O_4 dSCDs is caused by the significant differences in the aerosol extinction magnitude on both days. However, the magnitude of the O_4 dSCDs for the EA of 20° (D) is less influenced by changes in AOD and profile shapes. A similar effect was also observed by Clémer et al. [5]. They identified that high elevation angles ($>15°$) are rather insensitive to small AOD changes (<0.15, 360 nm) when using exponentially decreasing profiles with SH from 0.25 to 0.75 km. It is apparent from this figure that the simulated O_4 dSCDs assuming aerosol extinction located in the BL are consistently lower than the measurements. The correlation under such conditions is always below the 1:1 line, or even below the x0.8 line. In particular, the exponential decrease with a SH=0.5 km shows the largest differences. On the other hand, the O_4 dSCDs are overestimated if the aerosol extinction is assumed to be only aloft (red circles), in particular in the low EAs. The comparison improves significantly and consistently for all EAs if the simulations are performed using the extinction profiles retrieved with the HSRL-2 (filled blue circles). In this case, the measured O_4 dSCDs are close to the 1:1 line for all EAs. A similar figure for 360 nm (with similar findings) can be found in the supporting information (Fig. S2).

The overall comparison between simulated and modeled O_4 dSCDs at both wavelengths, all EAs, both AAs, and both days is shown in Fig. 7. The O_4 dSCDs located in the lower left corner are from 17 July 2012 (high AOD); higher O_4 dSCDs correspond to low EAs on 22 July 2012 (low AOD,

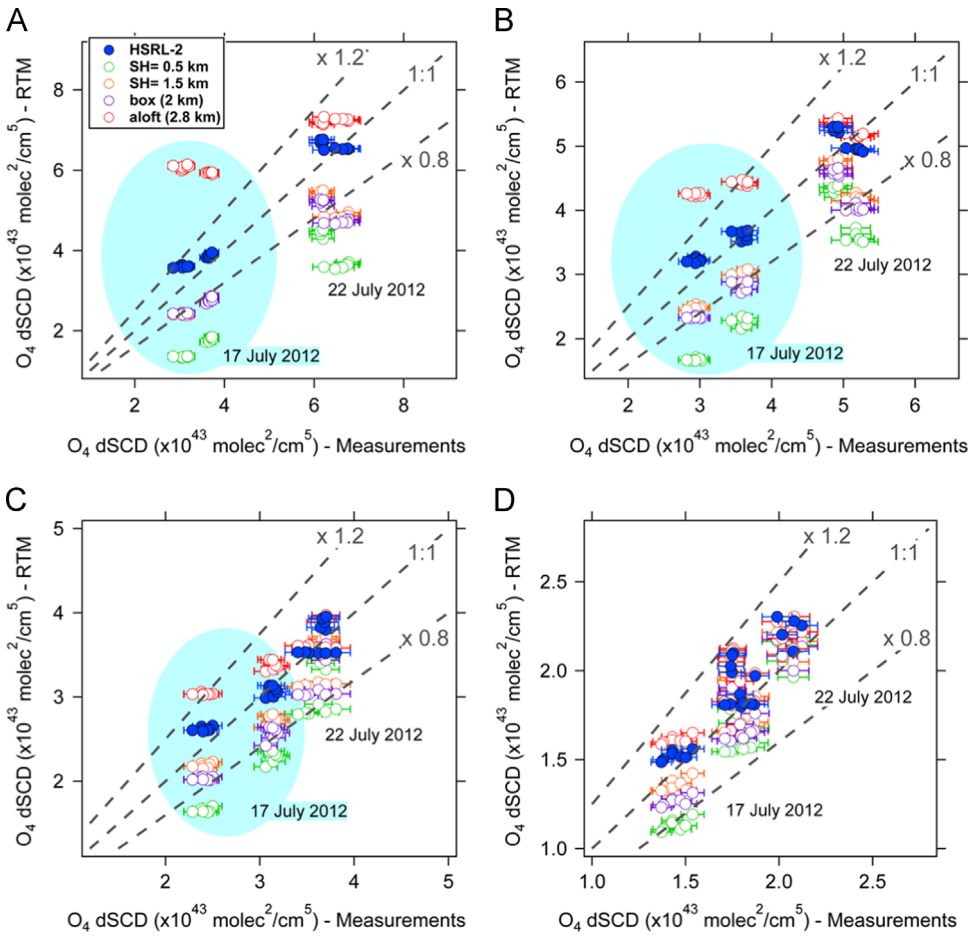

Fig. 6. Comparison of O_4 dSCDs measured and simulated at 477 nm for the elevation angles of (A) 3°, (B) 6°, (C) 10°, and (D) 20°. Note that the *x*-axis scales are different for each elevation angle. The light blue shaded oval represents values from 17 July, which are easily identified for low elevation angles ($\leq 10°$). For the elevation angle of 20° there is no apparent split in the O_4 dSCDs for the different days (the light blue shaded oval is not shown). The O_4 dSCD error bars in the measurements represent the 4% described in Section 2.1. (For interpretation of the references to color in this figure legend, the reader is referred to the web version of this article.)

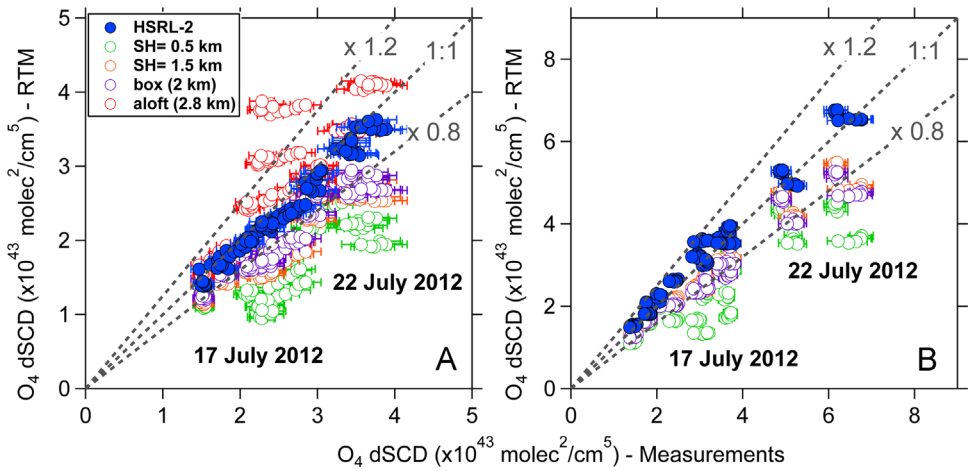

Fig. 7. Comparison of O_4 dSCDs measured and simulated at (A) 360 nm and (B) 477 nm. The correlation plot includes all the EAs with the extinction profiles shapes assumed and measured (Fig. 4.).

see Section 2.2). The overall qualitative evaluation confirms that the simulated O_4 dSCDs are underestimated if the assumption is made that aerosol extinction is located only in the BL; and the comparison improves if the extinction profiles retrieved with the HSRL-2 are used. We have noticed an AA dependency. In general, the southerly viewing angle contains smaller O_4 dSCDs that are closer to the 1:1 line if using the HSRL-2. On the other hand, the simulated northerly view yields slightly higher simulated O_4 dSCDs. This may be explained by the fact that we use average extinction profiles from the HSRL-2, and the instantaneous air mass measured by the 2-D-MAX-DOAS may be slightly different. However, the 1:1 line is within the error bars with averages of $6.4 \pm 0.4\%$ (360 nm) and $4.7 \pm 0.6\%$ (477 nm) if using the HSRL-2 measurements. For aerosol homogeneous conditions in the marine BL, Volkamer et al. [9] showed that comparison of measured and simulated O_4 SCD agreed within $1 \pm 2\%$ in the lower 400 m close to the surface when the aerosol extinction aloft is characterized by independent measurements under similar air masses.

A linear regression analysis was used to assess the effect of aerosol extinction profiles quantitatively for the different EAs. The different sets of simulated O_4 dSCDs were compared to the measurements with a two folded goal: (1) to identify a typical bias with the assumed extinction profiles and (2) to create a proxy for the CF_{O4} based on statistical analysis. To achieve the first goal the linear regression was calculated in the form $\boldsymbol{y}=m\boldsymbol{x}+b$ where $\boldsymbol{y}$ is the simulated and $\boldsymbol{x}$ is the measured O_4 dSCDs; m is the slope and b the intercept in $molec^2/cm^5$. The results of the linear correlation analysis using this approach are presented in Table 3. This Table shows the results among different EAs, for all EAs, and for the two wavelengths. Interestingly, the slope increases as the EA increases in all cases when the aerosol is assumed to be in the BL. This behavior is observed consistently at both wavelengths. In general, the offset (bias) is negative and higher than the O_4 dSCD error. These results suggest that the low EAs are highly sensitive towards aerosol layers aloft. This particular pattern is not observed if either the extinction profiles of the HSRL-2 or the aerosol assumed extinction aloft is used to initialize the RTM. Table 4 also shows the overall slopes and intercepts if data from all EAs are fitted simultaneously. Interestingly, the slope is smaller than unity when assuming aerosol extinction profiles in the BL. The overall correlation coefficients (R^2) improve significantly (0.98) by using the HSRL-2 extinction profiles with a slope close to unity. In general, the correlations decrease by assuming the extinction to be in the lower part of the atmosphere. This general approach to evaluate slopes and intercepts may potentially help future studies to better constrain elevated aerosol layers.

The quantitative estimation of the CF_{O4} was calculated by forcing the intercept to zero, i.e., linear model of $\boldsymbol{y}=m\boldsymbol{x}+0$ where the slope represents the proxy for the CF_{O4}. Results of this analysis are shown in Table 4. In general, the correlation using all EAs reveal that CF_{O4} between 0.65 and 0.85 are needed when the assumed extinction is located in the BL. One interesting finding is that for these conditions at lower EA a lower CF_{O4} is needed. This is contrary to findings by Irie et al. [18] where they show lower CF_{O4} values at higher EAs and with the empirical form of 1 – EA/60. However, Irie et al. [18] pointed out that uplifted aerosol layers were not observed using ground-based Lidar. Interestingly, they found good

Table 3
Results from the linear correlation analysis of the simulated and measured O_4 dSCDs using the EAs of 3°, 6°, 10°, 20° and the aerosol extinction profiles from Fig. 3. The analysis is performed using the linear model $y=mx+b$, where m is the slope and b the intercept.

Profile shape	EA (°)	Slope (360/477 nm)	Intercept $\times 10^{43}$ molec^2 cm^{-5} (360/477)	R^2 (360/477 nm)
Exp decrease (SH=0.5 km)	3	$0.77 \pm 0.05/0.78 \pm 0.06$	$-0.76 \pm 0.15/-1.02 \pm 0.27$	0.92/0.90
	6	$1.10 \pm 0.07/1.03 \pm 0.08$	$-1.34 \pm 0.20/-1.35 \pm 0.34$	0.92/0.88
	10	$1.27 \pm 0.07/1.19 \pm 0.09$	$-1.42 \pm 0.18/-1.28 \pm 0.28$	0.93/0.89
	20	$1.26 \pm 0.10/1.48 \pm 0.12$	$-0.73 \pm 0.18/-0.98 \pm 0.20$	0.86/0.88
	3, 6, 10, 20	$0.53 \pm 0.05/0.59 \pm 0.04$	$0.34 \pm 0.13/0.37 \pm 0.14$	0.53/0.73
Exp decrease (SH=1.5 km)	3	$0.80 \pm 0.04/0.81 \pm 0.04$	$-0.34 \pm 0.12/-0.09 \pm 0.22$	0.95/0.94
	6	$0.95 \pm 0.05/0.90 \pm 0.06$	$-0.56 \pm 0.16/-0.17 \pm 0.27$	0.93/0.90
	10	$1.00 \pm 0.06/0.97 \pm 0.07$	$-0.57 \pm 0.15/-0.20 \pm 0.23$	0.93/0.90
	20	$1.03 \pm 0.09/1.22 \pm 0.11$	$-0.34 \pm 0.17/-0.39 \pm 0.20$	0.83/0.83
	3, 6, 10, 20	$0.70 \pm 0.03/0.75 \pm 0.02$	$0.14 \pm 0.07/0.39 \pm 0.08$	0.88/0.93
Box (2 km)	3	$0.79 \pm 0.03/0.75 \pm 0.04$	$-0.14 \pm 0.11/0.10 \pm 0.20$	0.95/0.94
	6	$0.93 \pm 0.05/0.90 \pm 0.07$	$-0.46 \pm 0.14/-0.33 \pm 0.28$	0.94/0.89
	10	$1.05 \pm 0.06/1.02 \pm 0.08$	$-0.61 \pm 0.15/-0.47 \pm 0.25$	0.93/0.89
	20	$1.10 \pm 0.09/1.30 \pm 0.11$	$-0.38 \pm 0.17/-0.60 \pm 0.19$	0.85/0.87
	3, 6, 10, 20	$0.71 \pm 0.02/0.73 \pm 0.02$	$0.22 \pm 0.06/0.34 \pm 0.07$	0.90/0.94
Aloft (2.8 km)	3	$0.24 \pm 0.02/0.38 \pm 0.02$	$3.21 \pm 0.05/4.76 \pm 0.11$	0.90/0.94
	6	$0.39 \pm 0.02/0.48 \pm 0.03$	$2.17 \pm 0.06/2.81 \pm 0.13$	0.94/0.92
	10	$0.52 \pm 0.03/0.57 \pm 0.05$	$1.35 \pm 0.09/1.65 \pm 0.14$	0.92/0.88
	20	$0.73 \pm 0.09/0.92 \pm 0.11$	$0.45 \pm 00.16/0.31 \pm 0.19$	0.74/0.77
	3, 6, 10, 20	$1.01 \pm 0.07/1.05 \pm 0.06$	$0.30 \pm 0.18/0.57 \pm 0.22$	0.69/0.77
HSRL-2	3	$1.00 \pm 0.04/0.92 \pm 0.03$	$-0.16 \pm 0.12/0.66 \pm 0.12$	0.97/0/97
	6	$0.96 \pm 0.04/0.88 \pm 0.05$	$-0.06 \pm 0.12/0.58 \pm 0.21$	0.96/0.93
	10	$0.94 \pm 0.04/0.87 \pm 0.06$	$-0.01 \pm 0.12/0.48 \pm 0.19$	0.95/0.91
	20	$0.89 \pm 0.09/1.07 \pm 0.11$	$0.10 \pm 0.16/-0.01 \pm 0.19$	0.81/0.82
	3, 6, 10, 20	$0.94 \pm 0.01/0.99 \pm 0.02$	$0.01 \pm 0.04/0.18 \pm 0.06$	0.98/0.98

Table 4
Same as Table 3 but forcing the intercept to zero, i.e., linear model of $y=mx+0$.

Profile shape	EA (°)	Slope (CF_{O4}) (360/477 nm)	R^2 (360/477 nm)
Exp decrease (SH=0.5 km)	3	$0.54\pm0.01/0.58\pm0.02$	0.45/0.51
	6	$0.65\pm0.020/0.72\pm0.02$	0.33/0.43
	10	$0.74\pm0.02/0.80\pm0.02$	0.32/0.40
	20	$0.85\pm0.11/0.92\pm0.02$	0.39/0.35
	3, 6, 10, 20	$0.65\pm0.01/0.68\pm0.02$	0.80/0.97
Exp decrease (SH=1.5 km)	3	$0.70\pm0.01/0.80\pm0.01$	0.71/0.90
	6	$0.76\pm0.01/0.86\pm0.01$	0.60/0.82
	10	$0.80\pm0.01/0.91\pm0.01$	0.58/0.79
	20	$0.84\pm0.01/1.00\pm0.02$	0.55/0.56
	3, 6, 10, 20	$0.75\pm0.01/0.85\pm0.01$	1.02/1.19
Box (2 km)	3	$0.74\pm0.01/0.77\pm0.01$	0.85/0.99
	6	$0.78\pm0.010.83\pm0.02$	0.67/0.74
	10	$0.82\pm0.01/0.87\pm0.01$	0.57/0.65
	20	$0.89\pm0.01/0.97\pm0.02$	0.55/0.48
	3, 6, 10, 20	$0.78\pm0.01/0.82\pm0.01$	1.11/1.17
Aloft (2.8 km)	3	$1.24\pm0.04/1.29\pm0.06$	24.80/11.16
	6	$1.10\pm0.04/1.13\pm0.03$	7.75/5.25
	10	$1.02\pm0.03/1.08\pm0.02$	3.58/3.17
	20	$0.98\pm0.01/1.09\pm0.01$	1.35/1.09
	3, 6, 10, 20	$1.12\pm0.02/1.05\pm0.01$	0.85/1.06
HSRL-2	3	$0.95\pm0.01/1.05\pm0.01$	0.97/1.25
	6	$0.94\pm0.01/1.02\pm0.01$	0.93/1.24
	10	$0.93\pm0.01/1.02\pm0.01$	0.91/1.24
	20	$0.95\pm0.01/1.07\pm0.01$	0.92/0.81
	3, 6, 10, 20	$0.94\pm0.01/1.04\pm0.01$	0.92/1.06

agreement between near-surface extinction values with independent measurements without correction factor, although higher residuals at high EAs ($>20°$). This is consistent with the way that aerosol layers above significantly impact the O_4 dSCDs measured with low EAs. This strong EA dependency in the CF_{O4} is not found if the RTM is constrained by the HSRL-2 extinction profiles.

Our results indicate that knowledge about the extinction profiles in the BL and aloft are important in order to draw conclusions about the simulation of O_4 dSCDs. Assuming the aerosol extinction to be purely in the BL in combination with the application of the CF_{O4} would yield good agreement with independent co-located AOD observation. However, the real aerosol extinction profiles would be different. On the other hand, if the CF_{O4} is not applied the AOD would be underestimated by up to 60% (depending on the CF_{O4}, i.e., depending on the aerosol profile shape). Furthermore, if the goal is to retrieve aerosol extinction in the near-surface layer using "corrected" O_4 dSCDs this would yield an overestimation of the aerosol extinction coefficients created by the misplacement of aerosols. In fact, Zieger et al. [17] compared the near-surface aerosol extinction coefficients retrieved by MAX-DOAS with in-situ measurements and found systematically higher MAX-DOAS values. As mentioned in that study, the presence of aerosols at higher altitudes might result in an overestimation of the lowest extinction values. This is also clear in the assumed extinction profiles from Fig. 5 where all the assumed extinction profiles have the same AOD but higher aerosol extinction coefficients close to the surface, in particular using the exponentially decreasing profiles. These findings are in agreement with independent airborne MAX-DOAS observations, where it has been shown that agreement between measured and simulated O_4 SCD is within $1\pm2\%$ error in the BL when aerosols aloft are well characterized independently [9].

3.2. Effect of elevated aerosol layers on O_4 dSCDs

Fig. 8 shows the comparison of O_4 dSCDs (measured and simulated at 477 nm) for EAs of (A) 3°, (B) 6°, (C) 10°, and (D) 20° using both the HSRL-2 aerosol extinction below 2 km ('BL only', red circles) and the aerosol extinction up to~7 km ('HSRL-2', blue circles). Filled circles represent the north and open circles the south AA. It is interesting to note that the lowest EAs (3° and 6°) show among the largest systematic differences. The predicted O_4 dSCDs are systematically higher when aerosols aloft are ignored. Virtually no effect of the elevated aerosol layers is only observed at EA of 10°. At EAs of 20° the elevated layers have the reverse effect compared to the low EAs, i.e., predicted O_4 dSCDs are either unchanged, or systematically lower when aerosols aloft are ignored. This is consistent with the primary effect of elevated aerosol layers being visible in the lower EAs, as shown by the linear correlation analysis in Section 3.1. An AA dependency is also captured in Fig. 8, which is shown as time series in Fig. S3 in the supplement. The comparison of the simulations reveals differences in the lower EAs at different AA, which is not seen in the higher EAs. Significantly smaller differences are observed for the view to the North if elevated layers are accounted for.

The results of the linear regression analysis between the simulated ('BL only') and measured O_4 dSCDs are presented in Table 5. The EA analysis is performed using the approach presented in Section 3.1. Columns 2 to 4 show the results of the linear model $y=mx+b$, while column 5 shows the CF_{O4} obtained with the statistical model of $y=mx+0$. In comparison with Table 3 (HSRL-2 case) the slope and intercept are not significant different at 360 and 477 nm, indicating maximal sensitivity to aerosols in the boundary layer. However, the CF_{O4} is significantly different for the EA of 3° and 6°, especially at 477 nm. In this case, the CF_{O4} is larger than 5% when the aerosols aloft are not taken into account. Overall, these results confirm that ground based observations of O4 dSCDs are suitable to identify elevated aerosol layers and that the sensitivity is enhanced at the visible wavelengths.

3.3. Literature context: frequency of occurrence of elevated aerosol layers

The elevated aerosol layers identified in this work are not unique of the two presented case studies. Berg et al. [21] examined in more detail the contribution of layers aloft to AOD during TCAP using six research flights carried out with HSRL-2. They found that elevated layers (from 2.64 km to the top of the HSRL-2~7 km) represented as much as 40% of the total AOD in the continental column. On the other hand, in the maritime column all of the AOD was associated with aerosol below 2.64 km. Furthermore, the occurrence of elevated aerosol layers was examined over the TCAP area using four years data from the Cloud-

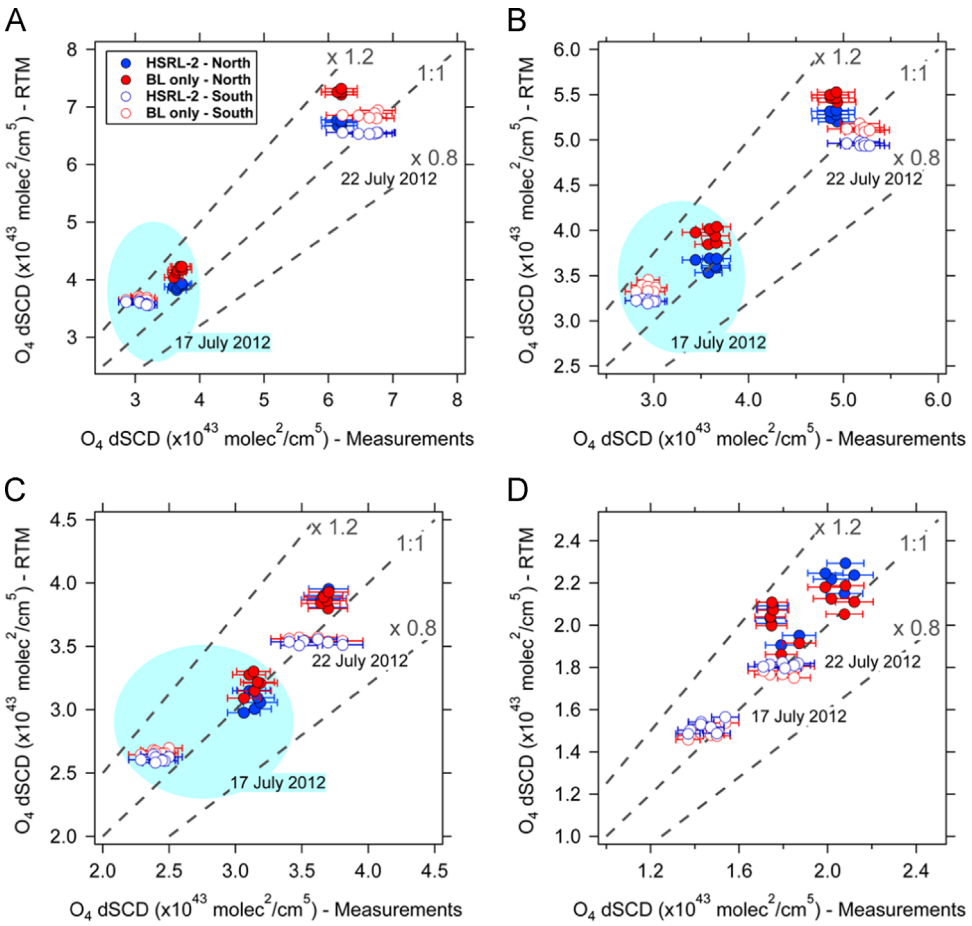

Fig. 8. Comparison of O_4 dSCDs measured and simulated at 477 nm for the EAs of (A) 3°, (B) 6°, (C) 10°, and (D) 20°. Red circles are assuming only HSRL-2 aerosol extinction below 2 km (extinction above 2 km was set to zero) and blue circles HSRL-2 aerosol extinction up to ~7 km. The north AA are solids while open circles represent the south AA. (For interpretation of the references to color in this figure legend, the reader is referred to the web version of this article.)

Table 5
Results from the linear correlation analysis of the simulated and measured O_4 dSCDs using the EAs of 3°, 6°, 10°, 20°, aerosol extinction profiles from 'BL only', and north and south AAs. The analysis is performed using the linear model $y=mx+b$ (columns 2 to 4) and $y=mx+0$ (column 5).

EA (°)	Slope (360/477 nm)	Intercept × 10^{43} molec^2 cm^{-5} (360/477)	R^2 (360/477 nm)	Slope (CF_{O4}) (360/477 nm)
3	1.02 ± 0.04/1.00 ± 0.04	−0.29 ± 0.12/0.54 ± 0.21	0.97/0.96	0.94 ± 0.01/1.11 ± 0.02
6	1.00 ± 0.04/0.88 ± 0.05	−0.15 ± 0.13/0.81 ± 0.20	0.96/0.94	0.96 ± 0.01/1.07 ± 0.02
10	0.91 ± 0.04/0.84 ± 0.05	0.12 ± 0.11/0.64 ± 0.15	0.95/0.93	0.95 ± 0.01/1.03 ± 0.01
20	0.80 ± 0.09/0.98 ± 0.13	0.23 ± 0.16/0.10 ± 0.20	0.76/0.77	0.94 ± 0.01/1.05 ± 0.01
3, 6, 10, 20	0.90 ± 0.01/1.06 ± 0.01	0.09 ± 0.01/0.10 ± 0.10	0.90/0.94	0.94 ± 0.01/1.06 ± 0.01

Aerosol Lidar and Infrared Pathfinder satellite (CALIPSO). In this long time series analysis more than 60% of the aerosol layer tops observed between 2 and 5 km are associated with layers aloft during the month of July. The importance of such layers was also noted by Goldstein et al. [44] in the Southeast of the U.S. They infer that much of the secondary organic aerosol must occur above the surface layer to explain the AOD in summer months. Recent studies using long time series from CALIPSO have shown that elevated layers are more frequent than expected [45–47].

The Intergovernmental Panel on Climate Change (IPCC) Working Group I of the Fifth Assessment Report summarizes the climatology of aerosol extinction vertical profiles globally, highlighting the importance of aerosol layers above 1 to 2 km [46]. They show that the average latitudinal vertical cross sections of the 532 nm aerosol extinction vertical profiles from CALIPSO during 2010 extended up to 4 km for the longitudinal bands of 20° W to 40° E and 60 to 120° E, especially for northerly latitudes (~0 to 50° N). Winker et al. [45] used six year data set from CALIPSO to characterize the global 3-dimensional distribution of tropospheric aerosols, and present evidence

that elevated aerosol layers (including the free troposphere) are important, and may be low-biased in the CALIPSO data. They compare HSRL extinction profiles co-located with CALIPSO overpasses in the eastern Caribbean, the Southeast US, and the mid-Atlantic region, and show that profiles obtained from CALIPSO are significantly lower (by about 0.002 km^{-1}) above 4 km altitude than the HSRL [45].

All past MAX-DOAS studies that applied the CF_{O4} (see Table 1) were conducted at northerly latitudes (between 35.0 to 52.0° N) and easterly longitudinal bands (between 4° to 117°E), where AOD is enhanced, and elevated aerosol layers are frequent [45,46]. According with the zonal mean distribution of aerosol extinction profiles obtained by Winker et al. [45] about 63% and 90% of the AOD extend roughly to about 1.5 and 3.0 km, respectively at north latitudes, i.e., a significant fraction of AOD is located above 1.5 km (~37% on average). During TCAP as much as 40% of AOD was located above 3 km. To the best of our knowledge elevated aerosol layers were not accounted for in the a-priori aerosol profiles used by previous MAX-DOAS studies that found a need for CF_{O4}.

3.4. Factors influencing the CF_{O4} with MAX-DOAS

In order to investigate the different factors that contribute to the CF_{O4}, O_4 SCDs were simulated using McArtim for four cases that differ in the assumptions about the temperature, pressure and aerosol profile. The assumptions for each of the four cases are listed in Table 6. All O_4 SCDs were simulated at 477 nm using the geometry of the EA scan performed with the 2-D-MAX-DOAS during TCAP. The simulations were carried out for conditions on 17 July (high AOD case study) and 22 July (low AOD case study), and the results are shown in Fig. 9. Cases 1 and 2 represent the atmospheric conditions as characterized by the radiosondes, while cases 3 and 4 assume the temperature and pressure profile of the U.S standard atmosphere. Fig. S4 shows the comparison of the temperature and O_4 concentration profiles using the measured and U.S standard atmospheric conditions for 17 July 2012. Below 13 km the measured temperature is 10–12 K larger than that of the U.S standard atmosphere. As a consequence, the O_4 concentration is 15–18% higher at a given altitude in the U.S standard atmosphere. Several previous MAX-DOAS studies assumed the U.S standard atmosphere directly and/or use ambient local surface conditions to adjust the U.S standard atmosphere profiles to represent the O_4 profile in the RTM [5,14–19]. Cases 1 and 3 use the measured HSRL-2 aerosol profile, while cases 2 and 4 use the same AOD confined to the lower atmosphere (exponential decreasing profile with a SH of 0.5 km, see Fig. 5). We can assume case 1 approximates well the measured O_4 dSCDs, because we have shown in Section 3.1 that under known aerosol distributions and air density profiles there is no need for CF_{O4}, and O_4 can be predicted with little error ($<0.1\%$) if the temperature and pressure profiles are known [2]. Fig. 9 compares case 2 (red), case 3 (blue), and case 4 (green) relative to case 1.

Fig. 9 shows three sets of analysis each for the 17 July (AOD ~ 0.35, top row) and 22 July (AOD < 0.10, bottom row): 1) O_4 SCDs in the zenith view (9A and 9D); 2) O_4 SCDs in the off-axis EAs (9B and 9E); and 3) O_4 dSCDs using the zenith reference spectrum of the same EA scan sequence. Surprisingly, the assumption about the aerosol distribution (case 2) does only have a very minor effect on the O_4 SCD, which increases by 4% for both case study days. On the other hand, if the U.S standard atmosphere is used (case 3) the O_4 SCDs is overestimated by ~18 and 13% on 17 and 22 July, respectively. This corresponds to an O_4 SCD offset (overestimate) of up to 0.1×10^{43} $molec^2\,cm^{-5}$. The axis scales of Fig. 9B and E are different on both case study days due to the difference in AOD. Interestingly, while points systematically fall above the 1:1 line in panels A and D (case 2), they fall systematically below the 1:1 line in panels B and E, and C and F. Similarly, the O_4 SCDs in the zenith view are higher for case 4 than for case 3, but lower for the off-axis angles. We conclude that independent of the assumptions about temperature and pressure conditions, a too low distribution of aerosols introduces a small but noticeable high bias in the zenith simulated O_4 SCDs, which translates in a small low-bias in the O_4 dSCDs for the off-axis EAs. This bias leads to $0.95 < CF_{O4} < 1$ for all cases and EAs. We conclude that the bias of the aerosol profile on the zenith view is small compared to the assumptions about vertical distributions of 1) aerosols and 2) air density, which have a major influence on the interpretation of the off-axis EAs.

If the aerosol is confined to the BL (case 2) CF_{O4} is needed at all EAs, especially at high AOD (see Table 4). Interestingly, using the U.S standard atmosphere increases the simulated O_4 SCDs for no good reason. This leads to a partial compensation of the bias created by the erroneous aerosol profile, and a smaller apparent deviation from the 1:1 line for both case study days, and at all EAs (but zenith). The assumption about the aerosol being confined in the BL (case 2) yields a negative bias that is significantly larger than the bias caused by the assumptions about air density (case 3). Recent studies that have used actual measurements of temperature, pressure and humidity profiles in the RTM did not find a need for CF_{O4} [9,19]. If RTM simulations use the U.S standard atmosphere, the bias in the predicted O_4 dSCDs depends on the relative difference of the local temperature and pressure conditions at the time of measurement to the conditions in the U.S standard atmosphere, which is often not known for studies in Table 1. This complicates an assessment of the causes for CF_{O4} in past MAX-DOAS studies. However, it is clear from Fig. 9 that the effect of misrepresenting the aerosol profile is especially important for EA < 20°. Notably, cases 3 and 4 also yield O_4 SCDs above the 1:1 line, but only for EAs ≥ 20°. We conclude that for EA < 20° the negative bias from assuming aerosols to be confined to the BL is more important than the assumption about the atmospheric air density profile.

3.5. Outlook

Ground based MAX-DOAS measurements of O_4 are mostly sensitive to aerosol in the boundary layer. However, the results of this study indicate that such measurements are affected by the presence of aerosol layers aloft. As a consequence, even O_4 dSCDs measured in the lower EA

contain bias caused by elevated aerosol layers, which has potential to translate into bias of partial AOD that is attributed to the BL based on O_4 dSCDs alone. Elevated aerosol layers were identified primarily with the visible wavelengths. In order to ovoid bias in the simulation of O_4 dSCDs we recommend the use of actual temperature and pressure vertical profiles in the RTM [9,19,48,49].

Under known atmospheric conditions of temperature and pressure we propose that the pattern of EA-dependent O_4 dSCD offsets can be systematically exploited to help characterize aerosol extinction aloft with ground-based MAX-DOAS, and possibly better characterize these elevated layers. An initial step may be to use total AOD from external sources, e.g., from measurements of the Raman Scattering Probability with the same instrument [50] or independent direct-sun observations (e.g, AERONET) and perform the linear correlation analysis as presented in this work. Friess et al. [4] had developed a non-linear inversion based on synthetic spectra and found that O_4 dSCDs are sensitive to aerosol layers located about ~3 km altitude. They had suggested that the information content is enhanced when the non-linear retrieval inversion uses O_4 dSCDs measured at different wavelengths simultaneously.

Table 6
Atmospheric and aerosol conditions used in four case sensitivity tests to simulate O_4 SCDs.

Case	Atmosphere	Aerosol
1	Radiosonde	HSRL-2
2	Radiosonde	Exponential (SH=0.5 km)
3	U.S atmosphere	HSRL-2
4	U.S atmosphere	Exponential (SH=0.5 km)

Our results support such sensitivity, which exists at any single O_4 band but mostly at visible wavelengths. The simultaneous use of wavelength dependent O_4 dSCD offsets, optimized viewing geometries, and external constraints to AOD is promising to maximize information to characterize layers aloft. The retrieval of aerosol extinction profiles and partial AODs in the boundary layer and free troposphere, especially elevated aerosol layers, deserves further investigation. The TCAP dataset provides a unique opportunity to apply, further develop and test state-of-the-art retrievals of elevated aerosol layers. The data of the two case studies described here is available for collaborative studies upon request from the authors.

Finally, to develop a complete picture about the need for CF_{O4} with ground-based MAX-DOAS, a study in the absence of elevated aerosol layers, that has aerosols confined to the BL and benefits from collocated independent quantitative measurements of highly vertically resolved and multispectral aerosol extinction profiles and atmospheric conditions remains desirable.

4. Summary and conclusions

We have presented a detailed study of the simulation of O_4 dSCDs under conditions when the aerosol extinction profiles are well-known. We conclude the following:

- Excellent agreement is found between measurements and simulation of O_4 dSCDs using independently measured, highly vertically-resolved aerosol extinction profiles. A linear correlation has slope close to unity, no significant offset, and $R^2 > 0.98$. In particular, no

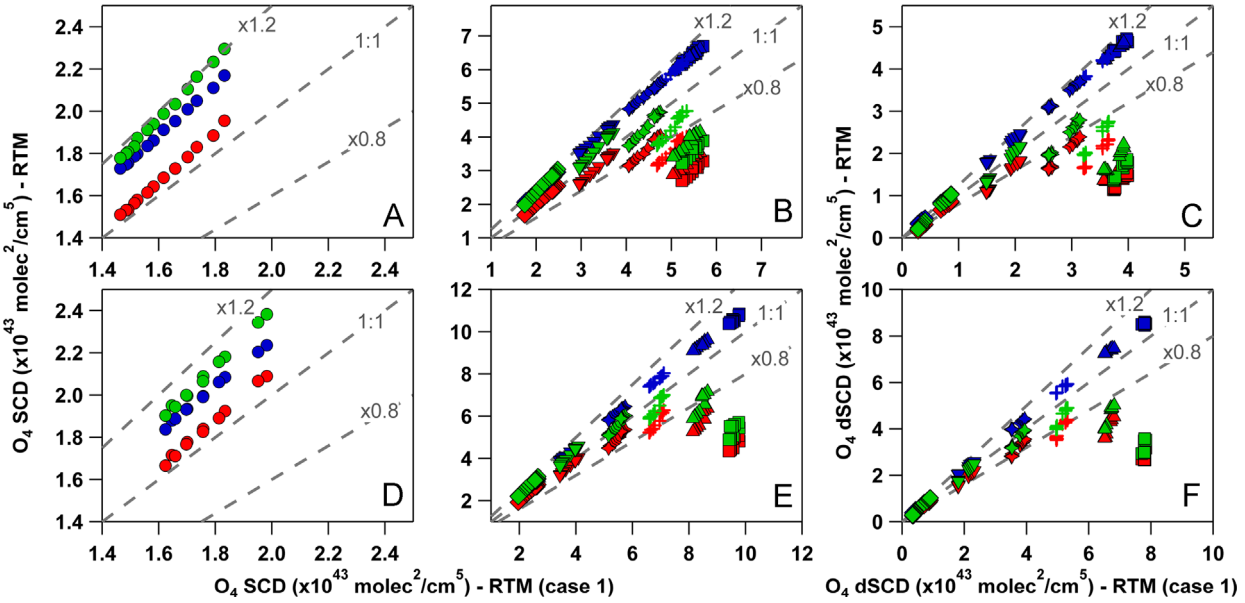

Fig. 9. Comparisons of the simulation of O_4 SCDs (A,B,D,E) and O_4 dSCDs (C,F) for case 2 (red), case 3 (blue), and case 4 (green) relative to case 1 (see Table 6) on (top row) 17 July and (bottom row) 22 July 2012. Different symbols mark different EAs: (circle) 90, (diamond) 45, (triangle down) 20, (star) 10, (plus) 6, (triangle) 3, and (square) 1 EA. (For interpretation of the references to color in this figure legend, the reader is referred to the web version of this article.)

evidence for CF_{O4} is found at 360 and 477 nm, under conditions of high and low AOD.

- The dominant fraction of the AOD (between 47% and 68%) was present in form of elevated aerosol layers. Although maximum sensitivity is achieved close to the surface we show that even for low AOD (near molecular scattering dominant conditions), ground-based O_4 dSCD measurements, mainly at 477 nm and low EAs, show sensitivity to such elevated aerosol layers. When elevated aerosol layers are present and total AOD is used in the boundary layer to constrain O_4 simulations a slope that is consistently smaller than unity (0.53–0.75), and an offset that is greater than the O_4 dSCD errors of 1.80×10^{42} molec^2/cm^5 for the 360 nm and 1.45×10^{42} molec^2/cm^5 for the 477 are found. A proxy for the CF_{O4} is estimated, and the range of CF_{O4} is found to be consistent with values that have been reported in recent MAX-DOAS studies.
- An EA analysis revealed a consistent and significant negative bias in the O_4 dSCD simulations for all EAs if AOD is high and aerosol distributions are confined to near the surface. The same effect is found when the AOD is small (AOD < 0.1 at 477 nm), however only for EA $< 10°$. If the EA-dependent bias (intercept in Table 3) is ignored, this manifests as a systematic EA dependence of CF_{O4} that is most pronounced in the lowest EAs, and equivalent to an overestimation of near-surface extinction.
- We propose that the pattern of EA-dependent O_4 dSCD offsets can be systematically exploited in combination with external constraints to AOD to better characterize these elevated layers with ground-based MAX-DOAS.
- The aerosol layers aloft identified in this work were not a peculiarity of the two case studies we have selected to investigate, but were frequently observed in a period of four years in the Cape Cod bay area [21]. Future studies might need to consider the impact of such layers on the scattering of sunlight as seen by ground-based passive remote sensing instruments.

There is now consistent evidence from MAX-DOAS, DS-DOAS and AMAX-DOAS measurements [9,19] that suggests CF_{O4} are small or not needed if there is enough information about aerosols. A recent study has shown that there is no fundamental limitation on using O_4 dSCDs to constrain aerosol extinction profiles from aircraft [9]. O_4 simulations need to take into account the possibility of elevated aerosol layers. Unless they are accounted for, elevated aerosol layers can result in the overestimation of extinction coefficients near the surface. The retrieval of aerosol profiles by MAX-DOAS is not limited to O_4, and is particularly promising if O_4 is combined with other parameters that constrain AOD, such as the Raman scattering probability [14,50]. The implication of elevated aerosol layers for the interpretation of other trace gases deserves further investigation.

Acknowledgments

The 2-D-MAX-DOAS instrument was developed with support from the NSF-CAREER award ATM-0847793, and US Department of Energy (DoE) award DE-SC0006080 supported the TCAP deployment. Ivan Ortega is recipient of a NASA Earth Science graduate fellowship. The authors are grateful to Tim Deutschmann for providing support with the McArtim RTM. The authors thank the entire TCAP team for their support during the campaign. We further thank Rick Wagener and Laurie Gregory for providing the AERONET data, Gary Hodges and Kathy Lantz for providing the NOAA MFRSR data, Caroline Fayt and Michel van Roozendael for providing the WinDOAS software, and Thomas Wagner for helpful discussions.

Appendix A. Supplementary material

Supplementary data associated with this article can be found in the online version at http://dx.doi.org/10.1016/j.jqsrt.2016.02.021.

References

[1] Greenblatt GD, Orlando JJ, Burkholder JB, Ravishankara AR. Absorption measurements of oxygen between 330 and 1140 nm. J Geophys Res 1990;95:18577–82. http://dx.doi.org/10.1029/JD095iD11p18577.

[2] Thalman R, Volkamer R. Temperature dependent absorption cross sections of O_2–O_2 collision pairs between 340 and 630 nm and at atmospherically relevant pressure. Phys Chem Chem Phys 2013;15(37):15371–81. http://dx.doi.org/10.1039/c3cp50968k.

[3] Wagner T, Dix B, Friedeburg C v, Friess U, Sanghavi S, Sinreich R, Platt U. MAX-DOAS O_4 measurements: a new technique to derive information on atmospheric aerosols-Principles and information content. J Geophys Res (Atmos) 2004;109:D22205. http://dx.doi.org/10.1029/2004JD004904.

[4] Friess U, Monks PS, Remedios JJ, Rozanov A, Sinreich R, Wagner T, Platt U. MAX-DOAS O_4 measurements: a new technique to derive information on atmospheric aerosols: 2. Modeling studies. J Geophys Res (Atmos) 2006;111:D14203. http://dx.doi.org/10.1029/2005JD006618.

[5] Clémer K, Van Roozendael M, Fayt C, Hendrick F, Hermans C, Pinardi G, Spurr R, Wang P, De Maziere M. Multiple wavelength retrieval of tropospheric aerosol optical properties from MAXDOAS measurements in Beijing. Atmos Meas Tech 2010;3(4):863–78, http://dx.doi.org/10.5194/amt-3-863-2010.

[6] Sinreich R, Merten A, Molina L, Volkamer R. Parameterizing radiative transfer to convert MAX-DOAS dSCDs into near-surface box-averaged mixing ratios. Atmos Meas Tech 2013;6:1521–32, http://dx.doi.org/10.5194/amt-6-1521-2013.

[7] Melamed ML, Langford AO, Daniel JS, Portmann RW, Miller HL, Eubank CS, Schofield R, Holloway J, Solomon S. Sulfur dioxide emission flux measurements from point sources using airborne near ultraviolet spectroscopy during the new England air quality study 2004. J Geophys Research: Atmos 2008;113(D2). http://dx.doi.org/10.1029/2007JD008923.

[8] Baidar S, Oetjen H, Coburn S, Dix B, Ortega I, Sinreich R, Volkamer R. The CU airborne MAX-DOAS instrument: vertical profiling of aerosol extinction and trace gases. Atmos Meas Tech 2013;6(3):719–39. http://dx.doi.org/10.5194/amt-6-719-2013.

[9] Volkamer R, Baidar S, Campos TL, Coburn S, DiGangi JP, Dix B, Eloranta EW, Koenig TK, Morley B, Ortega I, Pierce BR, Reeves M, Sinreich R, Wang S, Zondlo MA, Romashkin PA. Aircraft measurements of BrO, IO, glyoxal, NO_2, H_2O, O_2O_2 and aerosol extinction profiles in the tropics: comparison with aircraft-/ship-based in situ and lidar measurements. Atmos Meas Tech 2015;8(5):2121–48. http://dx.doi.org/10.5194/amt-8-2121-2015.

[10] Coburn S, Ortega I, Thalman R, Blomquist B, Fairall CW, Volkamer R. Measurements of diurnal variations and eddy covariance (EC) fluxes of glyoxal in the tropical marine boundary layer: description of the fast LED-CE-DOAS instrument. Atmos Meas Tech 2014;7(10):3579–95. http://dx.doi.org/10.5194/amt-7-3579-2014.

[11] Acarreta JR, De Haan JF, Stammes P. Cloud pressure retrieval using the O_2–O_2 absorption band at 477 nm. J Geophys Res (Atmos) 2004;109:5204. http://dx.doi.org/10.1029/2003JD003915.

[12] Wagner T, Burrows JP, Deutschmann T, Dix B, von Friedeburg C, Friess U, Hendrick F, Heue K, Irie H, Iwabuchi H, Kanaya Y, Keller J,

McLinden J, Oetjen H, Palazzi E, Petritoli A, Platt U, Postylyakov O, Pukite J, Richter A, van Roozendael M, Rozanov A, Rozanov V, Sinreich R, Sanghavi S, Wittrock F. Comparison of box-air-mass-factors and radiances for Multiple-Axis Differential Optical Absorption Spectroscopy (MAX-DOAS) geometries calculated from different UV/visible radiative transfer models. Atmos Chem Phys 2007;7(7):1809–33.

[13] Rodgers CD. Inverse methods for atmospheric sounding: theory and practice. Singapore: World Scientific; 2000.

[14] Wagner T, Deutschmann T, Platt U. Determination of aerosol properties from MAX-DOAS observations of the Ring effect. Atmos Meas Tech 2009;2(2):495–512. http://dx.doi.org/10.5194/amt-2-495-2009.

[15] Irie H, Takashima H, Kanaya Y, Boersma KF, Gast L, Wittrock F, Brunner D, Zhou Y, Van Roozendael M. Eight-component retrievals from ground-based MAX-DOAS observations. Atmos Meas Tech 2011;4(6):1027–44. http://dx.doi.org/10.5194/amt-4-1027-2011.

[16] Vlemmix T, Piters AJM, Berkhout AJC, Gast LFL, Wang P, Levelt PF. Ability of the MAX-DOAS method to derive profile information for NO_2: can the boundary layer and free troposphere be separated? Atmos Meas Tech 2011;4(12):2659–84. http://dx.doi.org/10.5194/amt-4-2659-2011.

[17] Zieger P, Weingartner E, Henzing J, Moerman M, de Leeuw G, Mikkila J, Ehn M, Petaja T, Clémer K, van Roozendael M, Yilmaz S, Friess U, Irie H, Wagner T, Shaiganfar R, Beirle S, Apituley A, Wilson K, Baltensperger U. Comparison of ambient aerosol extinction coefficients obtained from in-situ, MAX-DOAS and lidar measurements at Cabauw. Atmos Chem Phys 2011;11(6):2603–24. http://dx.doi.org/10.5194/acp-11-2603-2011.

[18] Irie H, Nakayama T, Shimizu A, Yamazaki A, Nagai T, Uchiyama A, Zaizen Y, Kagamitani S, Matsumi Y. Evaluation of max-doas aerosol retrievals by coincident observations using crds, lidar, and sky radiometer intsukuba, japan. Atmos Meas Tech 2015;8(7). http://dx.doi.org/10.5194/amt-8-2775-2015.

[19] Spinei E, Cede A, Herman J, Mount GH, Eloranta E, Morley B, Baidar S, Dix B, Ortega I, Koenig T, Volkamer R. Ground-based direct-sun DOAS and airborne MAX-DOAS measurements of the collision induced oxygen complex, O_2O_2, absorption with significant pressure and temperature differences. Atmos Meas Tech 2015;8:793–809. http://dx.doi.org/10.5194/amt-8-793-2015.

[20] Remmers J, Wagner T. Azimuthal variability of trace gases and aerosols measured during the MADCAT campaign in summer 2013 in Mainz, Germany. In: Presentation at the 7th international DOAS workshop. Brussels; 6–8 July 2015.

[21] Berg LK, Fast JD, Barnard JC, Burton SP, Cairns B, Chand D, Comstock JM, Dunagan S, Ferrare RA, Flynn CJ, Hair JW, Hostetler CA, Hubbe J, Je_erson A, Johnson R, Kassianov EI, Kluzek CD, Kollias P, Lamer K, Lantz K, Mei F, Miller MA, Michalsky J, Ortega I, Pekour M, Rogers RR, Russell PB, Redemann J, Sedlacek AJ, Segal-Rosenheimer M, Schmid B, Shilling JE, Shinozuka Y, Springston SR, Tomlinson JM, Tyrrell M, Wilson JM, Volkamer R, Zelenyuk A, Berkowitz CM. The two-column aerosol project: phase i overview and impact of elevated aerosol layers on aerosol optical depth. J Geophys Research: Atmos 2015. http://dx.doi.org/10.1002/2015JD023848.

[22] Ortega I, Koenig T, Sinreich R, Thomson D, Volkamer R. The CU 2-D-MAX-DOAS instrument-Part 1: retrieval of 3-D distributions of NO_2 and azimuth-dependent OVOC ratios. Atmos Meas Tech 2015;8(6):2371–95. http://dx.doi.org/10.5194/amt-8-2371-2015.

[23] Platt U, Stutz J. Differential optical absorption spectroscopy: principles and applications. Heidelberg: Springer Verlag; 2008.

[24] Fayt C, Van Roozendael M. WinDOAS 2.1, software user manual, Belgian Institute for Space Aeronomy. Brussels, Belgium. Available at: ⟨http://UV–vis.aeronomie.be/software/windoas/windoas-sum-210b.pdf⟩; 2001 (last accessed 29 May 2012).

[25] Bogumil K, Orphal J, Homann T, Voigt S, Spietz P, Fleischmann O, Vogel A, Hartmann M, Kromminga H, Bovensmann H, Frerick J, Burrows J. Measurements of molecular absorption spectra with the SCIAMACHY pre-flight model: instrument characterization and reference data for atmospheric remote-sensing in the 230–2380 nm region. J Photochem Photobiol A-Chem 2003;157(2–3):167–84, http://dx.doi.org/10.1016/S1010-6030(03)00062-5.

[26] Vandaele A, Hermans C, Simon P, Carleer M, Colin R, Fally S, Merienne M, Jenouvrier A, Coquart B. Measurements of the NO_2 absorption cross-section from 42 000 cm^{-1} to 10 000 cm^{-1} (238-1000 nm) at 220 K and 294 K. J Quant Spectrosc Radiat Transf 1998;59(3–5):171–84. http://dx.doi.org/10.1016/S0022-4073(97)00168-4.

[27] Rothman L, Gordon I, Babikov Y, Barbe A, Benner DC, Bernath P, Birk M, Bizzocchi L, Boudon V, Brown L, Campargue A, Chance K, Cohen E, Coudert L, Devi V, Drouin B, Fayt A, Flaud J-M, Gamache R, Harrison J, Hartmann J-M, Hill C, Hodges J, Jacquemart D, Jolly A, Lamouroux J, Roy RL, Li G, Long D, Lyulin O, Mackie C, Massie S, Mikhailenko S, Mller H, Naumenko C, Nikitin A, Orphal J, Perevalov V, Perrin A, Polovtseva E, Richard C, Smith M, Starikova E, Sung K, Tashkun S, Tennyson J, Toon G, Tyuterev V, Wagner G. The HITRAN2012 molecular spectroscopic database. J Quant Spectrosc Radiat Transf 2013;130:4–50. http://dx.doi.org/10.1016/j.jqsrt.2013.07.002.

[28] Volkamer R, Spietz P, Burrows J, Platt U. High-resolution absorption cross-section of glyoxal in the UV–vis and IR spectral ranges. J Photochem Photobiol A-Chem 2005;172(1):35–46, http://dx.doi.org/10.1016/j.jphotochem.2004.11.011.

[29] Meller R, Moortgat G. Temperature dependence of the absorption cross sections of formaldehyde between 223 and 323 K in the wavelength range 225–375 nm. J Geophys Res-Atmos 2000;105(D6):7089–101. http://dx.doi.org/10.1029/1999JD901074.

[30] Fleischmann OC, Hartmann M, Burrows JP, Orphal J. New ultraviolet absorption cross-sections of bro at atmospheric temperatures measured by time-windowing fourier transform spectroscopy. J Photochem Photobiol A: Chem 2004;168(12):117–32. http://dx.doi.org/10.1016/j.jphotochem.2004.03.026.

[31] Kraus S. A framework design for doas; 2006.

[32] Grainger J, Ring J. Anomalous Fraunhofer line profiles. Nature 1962;193(4817):762. http://dx.doi.org/10.1038/193762a0.

[33] Hermans C. Measurement of absorption cross sections and spectroscopicmolecular parameters: O_2 and its collisional induced absorption. Available at: ⟨http://spectrolab.aeronomie.be/o2.htm⟩; 2002 (last accessed 29 May 2012).

[34] Hair JW, Hostetler CA, Cook AL, Harper DB, Ferrare RA, Mack TL, Welch W, Izquierdo LR, Hovis FE. Airborne high spectral resolution lidar for profiling aerosol optical properties. Appl Opt 2008;47(36):6734–52. http://dx.doi.org/10.1364/AO.47.006734.

[35] Grund CJ, Eloranta EW. University of Wisconsin high spectral resolution lidar. Opt Eng 1991;30(1):6–12. http://dx.doi.org/10.1117/12.55766.

[36] Muller D, Hostetler CA, Ferrare RA, Burton SP, Chemyakin E, Kolgotin A, Hair JW, Cook AL, Harper DB, Rogers RR, Hare RW, Cleckner CS, Obland MD, Tomlinson J, Berg LK, Schmid B. Airborne Multiwavelength High Spectral Resolution Lidar (HSRL-2) observations during TCAP 2012: vertical profiles of optical and microphysical properties of a smoke/urban haze plume over the northeastern coast of the US. Atmos Meas Tech 2014;7(10):3487–96. http://dx.doi.org/10.5194/amt-7-3487-2014.

[37] Bodhaine BA, Wood NB, Dutton EG, Slusser JR. On Rayleigh optical depth calculations. J Atmos Ocean Technol 1999;16:1854, http://dx.doi.org/10.1175/1520-0426(1999)016<1854:ORODC>2.0.CO;2.

[38] Harrison L, Michalsky J. Objective algorithms for the retrieval of optical depths from ground-based measurements. Appl Opt 1994;33(22):5126–32. http://dx.doi.org/10.1364/AO.33.005126.

[39] Holben B, Eck T, Slutsker I, Tanr D, Buis J, Setzer A, Vermote E, Reagan J, Kaufman Y, Nakajima T, Lavenu F, Jankowiak I, Smirnov A. AERONET a federated instrument network and data archive for aerosol characterization. Remote Sens Environ 1998;66(1):1–16. http://dx.doi.org/10.1016/S0034-4257(98)00031-5.

[40] Deutschmann T, Beirle S, Friess U, Grzegorski M, Kern C, Kritten L, Platt U, Prados-Roman C, Pukite J, Wagner T, Werner B, Pfeilsticker K. The Monte Carlo atmospheric radiative transfer model McArtim: Introduction and validation of Jacobians and 3D features. J Quant Spectrosc Radiat Transf 2011;112(6):1119–37. http://dx.doi.org/10.1016/j.jqsrt.2010.12.009.

[41] Kassianov E, Barnard J, Flynn C, Riihimaki L, Michalsky J, Hodges G. Areal-averaged spectral surface albedo from ground-based transmission data alone: toward an operational retrieval. Atmosphere 2014;5(3):597. http://dx.doi.org/10.3390/atmos5030597.

[42] Koelemeijer RBA, de Haan JF, Stammes P. A database of spectral surface reectivity in the range 335772 nm derived from 5.5 years of GOME observations. J Geophys Research: Atmos 2003;108(D2):4070. http://dx.doi.org/10.1029/2002JD002429.

[43] Dubovik O, Holben B, Eck TF, Smirnov A, Kaufman YF, King MD, Tanre D, Slutsker I. Variability of absorption and optical properties of key aerosol types observed in worldwide locations. J Atmos Sci 2002;59:590–608. http://dx.doi.org/10.1175/1520-0469(2002)059<0590:VOAAOP>2.0.CO;2.

[44] Goldstein AH, Koven CD, Heald CL, Fung IY. Biogenic carbon and anthropogenic pollutants combine to form a cooling haze over the southeastern United States. Proc Natl Acad Sci 2009;106(22):8835–40. http://dx.doi.org/10.1073/pnas.0904128106.

[45] Winker DM, Tackett JL, Getzewich BJ, Liu Z, Vaughan MA, Rogers RR. The global 3-D distribution of tropospheric aerosols as characterized by CALIOP. Atmos Chem Phys 2013;13(6):3345–61, http://dx.doi.org/10.5194/acp-13-3345-2013.

[46] Boucher O, Randall D, Artaxo P, Bretherton C, Feingold G, Forster P, Kerminen V-M, Kondo Y, Liao H, Lohmann U, Rasch P, Satheesh SK, Sherwood S, Stevens B, Zhang XY. Clouds and aerosols. In: Stocker

TF, Qin D, Plattner G-K, Tignor M, Allen SK, Boschung J, Nauels A, Xia Y, Bex V, Midgley PM, editors. Climate change 2013: the physical science basis. Contribution of working group I to the fifth assessment report of the intergovernmental panel on climate change. Cambridge, United Kingdom/New York, NY, USA: Cambridge University Press; 2013.

[47] Papagiannopoulos N, Mona L, Alados-Arboledas L, Amiridis V, Baars H, Binietoglou I, Bortoli D, D'Amico G, Giunta A, Guerrero-Rascado JL, Schwarz A, Pereira S, Spinelli N, Wandinger U, Wang X, Pappalardo G. Calipso climatological products: evaluation and suggestions from earlinet. Atmos Chem Phys Discuss 2015;15(21):31197–246, http://dx.doi.org/10.5194/acpd-15-31197-2015.

[48] Dix B, Baidar S, Bresch JF, Hall SR, Schmidt KS, Wang S, Volkamer R. Detection of iodine monoxide in the tropical free troposphere. Proc Natl Acad Sci USA 2013;110(6):2035–40, http://dx.doi.org/10.1073/pnas.1212386110.

[49] Wang S, Schmidt JA, Baidar S, Coburn S, Dix B, Koenig TK, Apel E, Bowdalo D, Campos TL, Eloranta E, Evans MJ, DiGangi JP, Zondlo MA, Gao R-S, Haggerty JA, Hall SR, Hornbrook RS, Jacob D, Morley B, Pierce B, Reeves M, Romashkin P, ter Schure A, Volkamer R. Active and widespread halogen chemistry in the tropical and subtropical free troposphere. Proc Natl Acad Sci USA 2015;112(30):9281–6. http://dx.doi.org/10.1073/pnas.1505142112.

[50] Ortega I, Coburn S, Berg LK, Lantz K, Michalsky J, Ferrare R, Hair J, Hostetler C, Volkamer R. The CU 2D-MAX-DOAS instrument-part 2: Raman scattering probability measurements and retrieval of aerosol optical properties. Atmos Meas Tech Discuss 2016. http://dx.doi.org/10.5194/amt-2015-385.